# Vacancy migration and accretion in Ni observed by perturbed $\gamma$-$\gamma$ angular correlations

Carl Allard, Gary S. Collins,* and Christoph Hohenemser
*Department of Physics, Clark University, Worcester, Massachusetts 01610*
(Received 13 May 1985)

Defect migration and accretion are observed in $^{111}$In-doped Ni, using perturbed $\gamma$-$\gamma$ angular correlations. Our samples were damaged by variable doses of proton irradiations and deformation at 200 K, well below resistivity stage III. Subsequent isochronal annealing extended to 900 K. When combined with previous work on ion-implanted Ni, the present work leads to a plausible recovery model in Ni which assumes vacancies migrate in stage III. The model includes the free migration and trapping of vacancy defects in the range $270 < T < 400$ K, enhanced diffusion and trapping of vacancy defects in the range $200 < T < 300$ K, and the formation of at least three, variable-sized multivacancy clusters above 350 K.

## I. INTRODUCTION

As indicated in several recent reviews,[1–4] perturbed $\gamma$-$\gamma$ angular correlations (PAC's) is a useful method for studying the migration and accretion of lattice defects in metals. Through the detection of hyperfine interaction frequencies, PAC provides unique "flagging" of individual defects trapped on dilute probe atoms injected into the lattice before or during the damage process.

In the present paper we are concerned with PAC studies of defect recovery in Ni, damaged below room temperature, using the $^{111}$In PAC probe. To achieve a fuller understanding of defect migration and trapping in the *Ni* $^{111}$In system, we present the first full account of results on samples damaged by proton irradiation and deformation below resistivity recovery stage III (300—470 K). The most distinctive feature of our measurements involves observation of at least three different combined-interaction sites. Thermal recovery of defects is monitored via isochronal annealing curves. We also investigated the dependence on dose of migration and trapping behavior. Using these and previous results for Ni, a plausible recovery model for stage III is proposed based on the assumption of vacancy migration in stage III. The model includes the free migration and trapping of monovacancies, divacancies, and trivacancies in the range $270 < T < 400$ K, enhanced diffusion and trapping of vacancies in the range $200 < T < 300$ K, and the formation of variable-sized multivacancy sites above 350 K. A preliminary discussion of our model has been given earlier.[5]

Extensive work based on other experimental methods provides the context for the present work, and some of it contributes explicitly to the recovery model we propose. In Table I we classify previous studies of defect recovery in Ni into eight categories, and indicate briefly the principal findings for each.[2,6–25] Thus, throughout resistivity recovery stage II ($70 < T < 300$ K), successively larger interstitital clusters migrate and accrete, vacancy clusters reorient, and impurities release trapped interstitials. In stage III (300—470 K), more than one vacancy species migrates, vacancy loops and clusters form, and smaller interstitial clusters are annihilated by migrating vacancies.

Earlier PAC studies suggest that trivacancies are freely migrant near 350 K.[20,26] What is not entirely clear is which other vacancy species migrate in stage III. In undertaking the present work it was therefore our goal to extend the PAC work to provide a better characterization of the vacancy species which migrate in stage III.

For reference, in Table II we summarize the *Ni* $^{111}$In defect sites observed in past PAC work,[20,21,27–34] including their hyperfine-interaction frequency, symmetry, and structural assignment, using the nomenclature of Pleiter and Hohenemser.[1] Sites S and C involve pure magnetic interactions, and were identified as defect-free substitutional $^{111}$In and a trivacancy trap complex with cubic symmetry. Two others, $B_1$ and the "high-frequency site," involve mixed magnetic-dipole—electric-quadrupole interactions, and were given a variety of interpretations, none well established. In the case of the "high-frequency site," the estimated quadrupole frequency $\omega_0$ and magnetic (Larmor) frequency $\omega_L$ have uncertainties of about a factor of 2 caused by the ill-defined character of mixed-interaction signals.

Experimental data reported here for the first time are variable-dose-irradiation and deformation studies, with initial damage induced at 200 K, well below stage III. In earlier irradiation and deformation work (see Table II) systematic dose dependences for all relevant defect species were not established.

## II. EXPERIMENTAL METHOD

In the PAC technique one studies the angular correlation of successive gamma rays in a $\gamma$-$\gamma$ cascade. In the present case we use the (171—245)-keV cascade which follows the decay of $^{111}$In. The first $\gamma$-ray establishes a quantization axis for the nucleus and creates an unequal population of magnetic sublevels in the intermediate state; as a result the second $\gamma$ ray has an anisotropic directional distribution with respect to the first, having the form

$$W(\theta) = 1 + A_2 P_2(\cos\theta) + \cdots , \quad (1)$$

where the ellipsis indicates negligible higher-order terms and where $\theta$ is the angle between the quantization axis

 

TABLE I. Recovery processes in nickel.

| Method | Stage II (70–300 K) | Stage III (300–470 K) | Selected references[a] |
|---|---|---|---|
| Resistivity recovery and stored energy release | Migration or breakup of interstitial ($i$) agglomerates; $2i$'s recover but do not dissociate | Free migration of at least two vacancy ($v$) species | 6–8 |
| Diffuse x-ray scattering | Motion and agglomeration of increasingly large $i$ clusters; transformation of $i$ agglomerates into loops upon accretion of more than 20–30 elementary defects | Continued agglomeration of $i$'s; migration and clustering of $v$'s | 9 |
| Magnetic and anelastic after effects | $v$ clusters reorient; dislocation motion; some free migration of defects; relase of trapped $i$'s from oversized impurities | Free migration of a defect with ⟨100⟩ symmetry near 365 K; migration of more than one species | 10–12 |
| Electron microscopy | | Agglomeration of $v$'s in loops; weak interaction of $v$'s with strain fields | 13,14 |
| Channeling | Migration of $i$ clusters; release[b] of trapped $i$'s from oversized impurities | $v$ migration and trapping at impurities; dissolution[b] of $i$ traps formed with undersized impurities | 15–17 |
| Positron annihilation | | Release of $i$'s or small $i$ clusters from impurity traps below 350 K; free migration of $v$'s above 350 K; trapping of $v$'s at impurities; nucleation of extended $v$ agglomerates by impurities | 18,19 |
| PAC and Mössbauer spectroscopies | Release[b] of trapped $i$'s from oversized impurities | $3v$ migration and trapping at In near 350 K; $1v$[b] and $2v$ migration and trapping at impurities | 2,20,21 |
| Computer simulation | | Free migration of $1v$, $2v$, and $3v$, with the $2v$ being most mobile; $nv$ clusters[b] with $n>4$ are immobile; dissolution[b] of $i$ trapped at undersized solutes | 22–24 |

[a]For a complete reference list, see Ref. 25.
[b]Observations made generally for fcc metals, but specific data for Ni are not available.

and the second $\gamma$ ray. In the presence of extranuclear perturbations, the directional distribution becomes time dependent. For randomly directed interactions it has the form

$$W(\theta,t)=1+A_2G_2(t)P_2(\cos\theta)+\cdots\ , \tag{2}$$

where $G_2(t)$ is known as the perturbation factor. Because in solids the extranuclear perturbations depend predominantly on the near-neighbor electronic environment, measurement of $G_2(t)$ may be used to "flag" specific lattice defects on probe atoms, and to distinguish these sites from substitutional probe atoms. It is in this way that PAC is used here to identify particular defect trap sites. Detailed treatments of the theory of perturbed angular correlations are available elsewhere.[35,36]

In our work on Ni we used a standard four-counter spectrometer with two background-corrected PAC spectra $C(\theta)$ measured at each of the angles $\theta=\pi$ and $\pi/2$. For data analysis we obtained the time-dependent ratio

$$\hat{G}_2(t)=\frac{2(k+1)}{3A_2\gamma_a}\frac{C(\pi)-C(\pi/2)}{C(\pi)+kC(\pi/2)}\ , \tag{3}$$

where $\gamma_a$ accounts for finite detector solid angle,[37] and $k=1$ or 2 as discussed below. Details of the setup and the relation between $G_2(t)$ and $\hat{G}_2(t)$ have been given elsewhere.[38] For the present purposes, three specific forms of $\hat{G}_2(t)$ are of interest:

(1) To describe lattice sites with pure magnetic interactions, resulting from a uniform hyperfine field $H_{\rm hf}$,

TABLE II. Summary of previous PAC work on $Ni^{111}In$.

| Site[a] | Coupling parameters[b] $\omega_0$ (Mrad/s) | $\langle hkl \rangle$ | $\eta$ | $\omega_L$ (Mrad/s) | Structural assignment[a] | Method of defect introduction[c] | References |
|---|---|---|---|---|---|---|---|
| S | ~0 | | | 98.2(3) | Substitutional | Imp.<br>Irr.<br>Def. | 21, 27–29[d]<br>30,31<br>20,32 |
| C | ~0 | | | 40(1) | Cubic symmetry trivacancy trap with interstitial In | Imp.<br>Irr.<br>Def. | 21,27,28<br>30,31<br>20,32 |
| $B_1$ | 53(5) | ⟨111⟩ | <0.2 | 39(5) | Divacancy trap with interstitial In, or faulted loop | Imp.<br>Irr.<br>Def. | 21,29,33,34<br>30 |
| High-frequency combined interaction | ~100 | | | ~100 | Other vacancy trap, or dislocation, or interstitials | Imp.<br>Irr.<br>Def. | 21<br>30,31<br>20,32 |

[a]Site nomenclature and structural assignments as discussed in Ref. 1.
[b]$\omega_0=(3\pi/10)eQV_{zz}/h$ is the quadrupole interaction frequency; $\langle hkl \rangle$ is the direction of the principal axis of the electric field gradient; $\eta$ is the asymmetry parameter for the electric field gradient; $\omega_L=\mu H_{hf}/\hbar I$ is the Larmor frequency.
[c]Abbreviations for method of defect introductions: Imp., implantation of $^{111}In$; Irr., irradiation; Def., deformation.
[d]In Ref. 29 measurements were made by $\beta$-$\gamma$ PAC after decay of $^{111}Ag$ through the same intermediate state, with $\omega_0=32(2)$ Mrad/s detected after room-temperature implantation.

directed perpendicular to the plane of the counters, we used $k=1$ in Eq. (3) and

$$\hat{G}_2(t)=\exp[-(2\sigma_L t)^2/2]\cos(2\omega_L t) \ , \quad (4)$$

where $\omega_L=\mu H_{hf}/I\hbar$ is the Larmor frequency, $\mu$ is the nuclear magnetic dipole moment, $I$ is the nuclear spin of the intermediate nuclear state, and $\sigma_L$ represents the width of the frequency distribution.

(2) To describe sites with pure electric-quadrupole coupling, and specifically for a randomly oriented, axially symmetric electric field gradient, we used $k=2$ and

$$\hat{G}_2(t)=\frac{1}{5}\left[1+\sum_{n=1}^{3} S_n \exp[-(n\sigma_Q t)^2/2]\cos(n\omega_0 t)\right] \ , \quad (5)$$

where $\omega_0=3\pi eQV_{zz}/10h$ is the coupling frequency of the nuclear quadrupole moment $Q$ in an electric field gradient with principal component $V_{zz}$, $\sigma_Q$ is the frequency distribution width, and the $S_n$ are known amplitude factors for the three frequency harmonics.

(3) To describe sites with combined magnetic-dipole and electric-quadrupole coupling, we used $k=2$ in Eq. (3) and fitted the time-dependent ratio to

$$\hat{G}_2(t)\simeq\exp[-(t/\Delta)^2]$$

near $t=0$, using $\Delta$ to parametrize the signal. Changes of $\Delta$ are used below to monitor transformations in combined-interaction sites. Use of such a phenomenological parameter is consistent with the fundamentally ambiguous character of combined-interaction sites for which $\omega_L\sim\omega_0$, as described by Pleiter.[39]

Figure 1 illustrates each of the three kinds of signals. The pure magnetic signal was obtained for substitutional

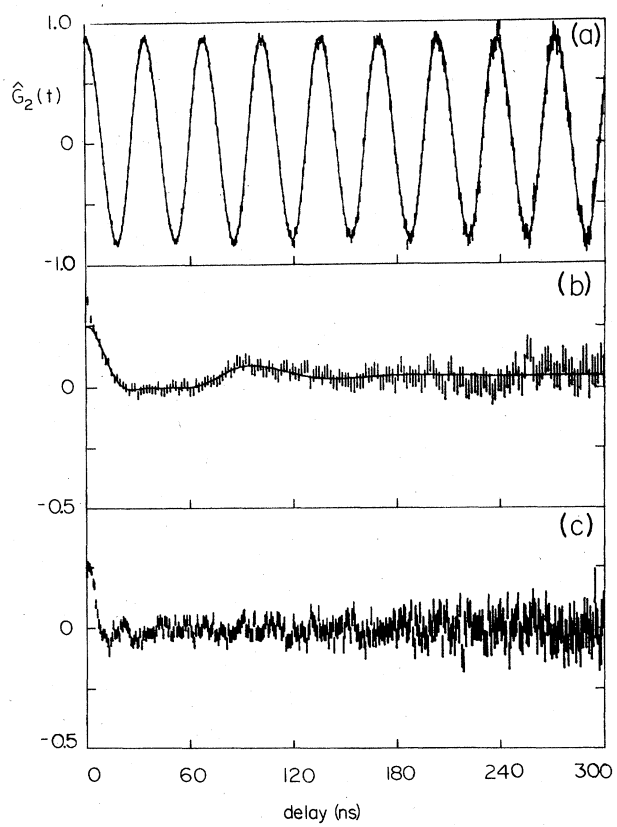


FIG. 1. Perturbation functions derived from PAC data. (a) Pure magnetic-dipole interaction in an undamaged sample. (b) Pure quadrupole signal obtained from Ni sample at 640 K which was deformed at room temperature. (c) Combined interaction after subtraction of the pure magnetic component in a sample deformed at room temperature.

$^{111}$In in Ni. The pure electric-quadrupole signal, which includes a distribution of frequencies $\omega_0$, was obtained for a defect complex from measurements made above the Curie temperature $T_C$. The combined-interaction signal was measured below $T_C$ for a different defect complex.

## III. EXPERIMENTAL RESULTS

### A. Irradiated Ni

Sources were made from 25-$\mu$m-thick, 99.998%-pure polycrystalline Ni foils, thinned to 6 $\mu$m by rolling, and subsequently annealed to remove rolling damage. Thinned foils were doped with carrier-free $^{111}$In (concentration $< 10^{-7}$ at. %) by electroplating from an acetone bath, diffusing at 1073 K for 1.5—2.0 h in a $H_2$ atmosphere, and rinsing in 1$M$ HCl for 15 s to remove surface In activity.

The irradiation-damage experiments performed in this work differ in two ways from previous work in our laboratory. Unlike studies by Suter *et al.*[30] and Allard *et al.*,[31] the *Ni* $^{111}$In samples were thinned enough to allow the 1.5-MeV proton beam to pass through them, thus avoiding high-density nuclear-stopping damage or the

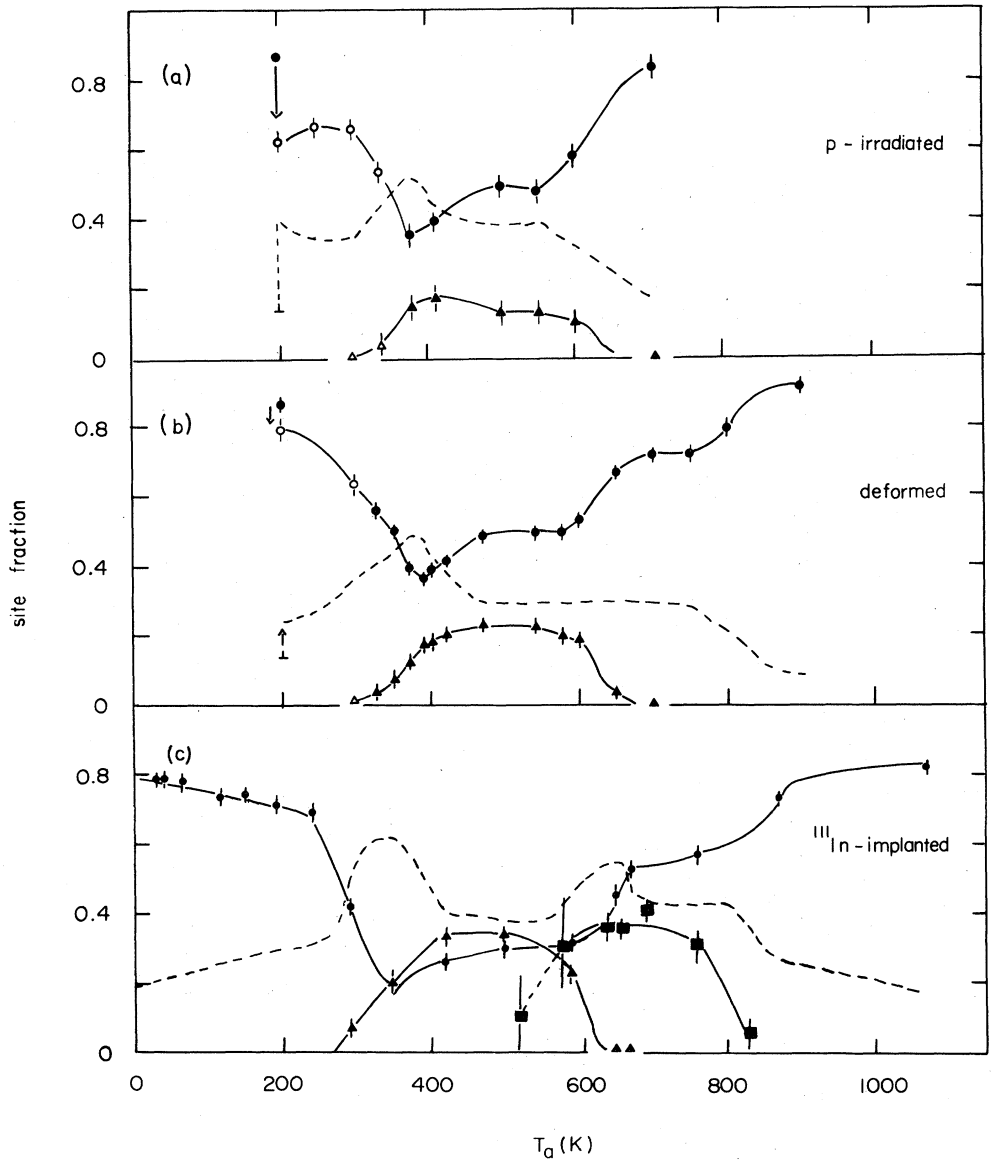


FIG. 2. $^{111}$In-site fractions in Ni during an isochronal annealing sequence after damage. The circles are the defect-free fraction; the triangles are the C site; the dashed line is the difference between these sites and unity, representing the total combined-interaction fraction. The squares in the bottom panel represent the $B_1$ defect as measured above $T_C$; the open and solid data points in the top two panels represent measurements at 77 and 297 K, respectively. (a) Sample irradiated at 200 K with 1.5-MeV protons to a dose of $17\times10^{15}$ $p/\text{cm}^2$. (b) Sample deformed to 20% area increase at 200 K. (c) Sample implanted with $^{111}$In at 10 K by Hohenemser *et al.* (Ref. 21).

possibility of hydrogen-defect interactions. Whereas the irradiations of Suter *et al.* were done at 300 K and those of Allard *et al.* at 77 K, the irradiations reported here were done at 200 K. This is below stage III and permits unambiguous observation of thermal migration in stage III, yet it is high enough to circumvent interstitial trapping during irradiation. Irradiation doses ranged from $6\times10^{14}$ to $170\times10^{14}$ $p/cm^2$.

All PAC data were obtained with the source foil polarized along its surface and perpendicular to the plane of the counters, using a small permanent magnet with a gap field of 3.5 kG. The sample and magnet were submerged in liquid $N_2$ when necessary. Before irradiation, typically 80% of the $^{111}$In atoms exhibited a pure magnet signal as shown in Fig. 1(a), whereas the remainder were associated with an undetectably high- or low-frequency mixed-interaction signal of uncertain origin (see below). Post-irradiation PAC measurements were conducted following isochronal anneals for 15 min over a range of temperatures. The anneals were performed in isopropyl alcohol baths below room temperature or in a vacuum oven above room temperature. Measurements were done in liquid $N_2$ or, when the annealing temperature was appreciably higher than 300 K, at room temperature.

Post-irradiation PAC spectra showed four distinct signals: two pure magnetic signals, identified clearly with substitutional $^{111}$In and the C site as in previous work (Table II), and two combined-interaction signals with decay times $\Delta$ of $\sim5$ and $\sim12$ ns, henceforth referred to as $MQ_1$ and $MQ_2$, respectively. The latter two signals are ill defined, and may or may not be the same as the "high-frequency" or $B_1$ sites reported earlier (Table II). Measured site fractions are shown in Fig. 2(a) as a function of annealing temperature. (In order to remove an irrelevant "background" signal due to defect-free probe atoms in the unirradiated parts of the samples, site fractions were corrected for the actual foil areas irradiated, which were smaller than the total foil areas.) The solid lines in Fig. 2(a) represent the amplitudes of the two directly measured magnetic signals, whereas the dashed line represents the sum of combined-interaction sites, obtained by subtracting the sum of the directly measured amplitudes from unity. The average fitted decay times for the combined-interaction sites are shown in Fig. 3(a) and a number of

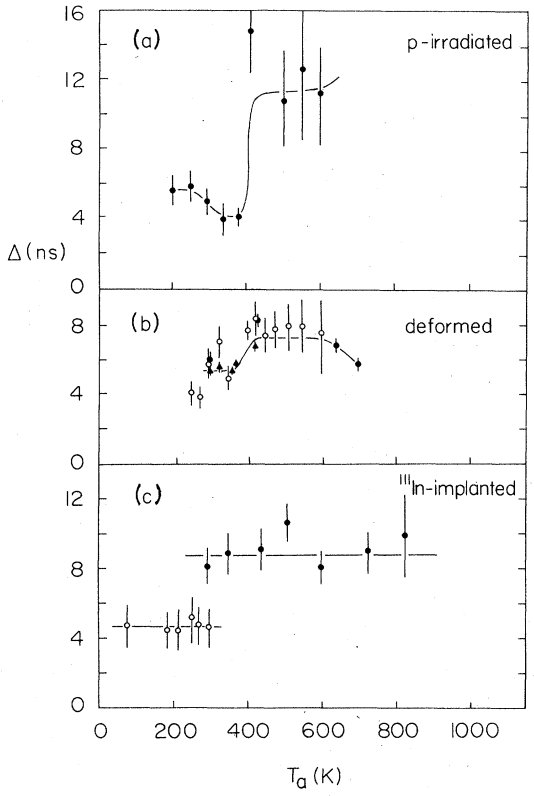


FIG. 3. Decay times $\Delta$ of the $^{111}$In combined-interaction signals as a function of annealing temperature of Ni sample after damage. (a) Sample irradiated with 1.5-MeV protons at 200 K to a dose of $17\times10^{15}$ $p/cm^2$. (b) Data for three different Ni samples deformed to area increases of 190% (open circles), 78% (solid circles), and 83% (triangles), at 200, 297, and 297 K, respectively. (c) Unpublished data by Pleiter and Hohenemser (Ref. 43) on Ni implanted at 77 K (open circles) and 297 K (solid circles).

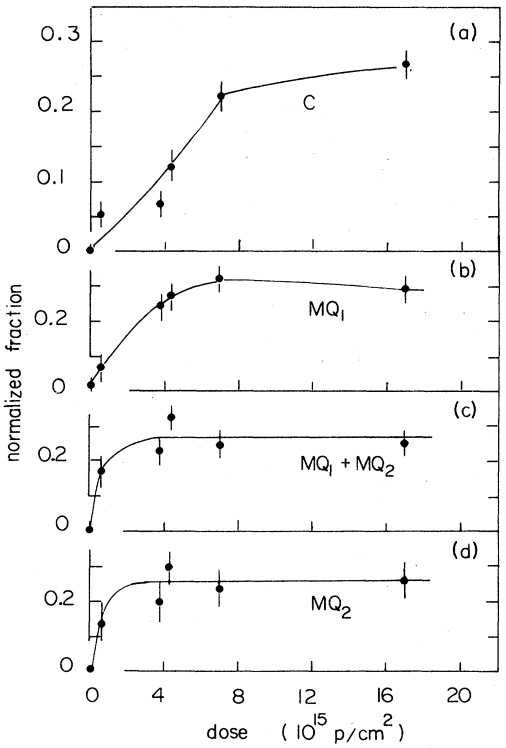


FIG. 4. Site fraction vs dose for polycrystalline Ni samples irradiated with 1.5-MeV protons at 200 K. (a) Maximum C-site fraction achieved throughout the annealing sequence, normalized by the defect-free fraction at 300 K. (b) $MQ_1$ fraction formed during irradiation, normalized by the defect-free fraction before irradiation. (c) The increase in the combined-interaction fraction upon annealing from room temperature to the temperature where the combined-interaction fraction is maximum, normalized by the defect-free fraction at room temperature. This quantity characterizes the trapping behavior of $MQ_1$ and $MQ_2$ between 300 and about 380 K (see text). (d) $MQ_2$ fraction at 500 K normalized by the defect-free fraction before irradiation.

dose dependences detected in trapping behavior are shown in Fig. 4. Examination of these results leads to the following observations.

(1) The C site forms thermally in the range 340—390 K and dissociates at 600—650 K [Fig. 2 (a)]. The maximum C-site population, observed for annealing temperatures in the range $400 < T_a < 600$ K, increases up to a dose of $\sim 8 \times 10^{15} p/\text{cm}^2$ and saturates thereafter [Fig. 4(a)].

(2) The combined-interaction site $MQ_1$, characterized by a mean decay time of $\Delta \sim 5$ ns, as shown in Fig. 3(a), traps athermally during irradiation [Fig. 2(a)] and detraps or is transformed in the range 380—410 K. The fraction of athermally trapped $MQ_1$ site increases up to a dose of $\sim 4 \times 10^{15} p/\text{cm}^2$ and saturated beyond [Fig. 4(b)]. (Because of the small value of $\Delta$, the amplitude of $MQ_1$ could not be determined directly with reliability, and was therefore deduced from the observed change in the substitutional fraction during irradiation.)

(3) The combined-interaction site $MQ_2$, characterized by a mean decay time $\Delta \sim 12$ ns, forms thermally between 350 and 410 K, and dissolves in the range of 600—700 K. Estimates of the amplitude of $MQ_2$, obtained by direct fitting of the signal, are shown in Fig. 5. (The absolute amplitude obtained in this way is sensitive to method of fitting and subject to a potential systematic error of $\pm 20\%$.)

(4) The total combined-interaction fraction, shown as a dashed line in Fig. 2(a) has a thermal trapping stage at 320—380 K. In contrast to the C site, the fraction of $^{111}$In involved in thermal trapping here appears to saturate at low dose [Fig. 4 (c)]. Additional analysis of variation of the mean decay time $\Delta$ indicated that both the $MQ_1$ and $MQ_2$ signals are present in that range of temperature.

(5) Two possible decompositions of the combined interaction sites are illustrated in Fig. 5. The first assumes

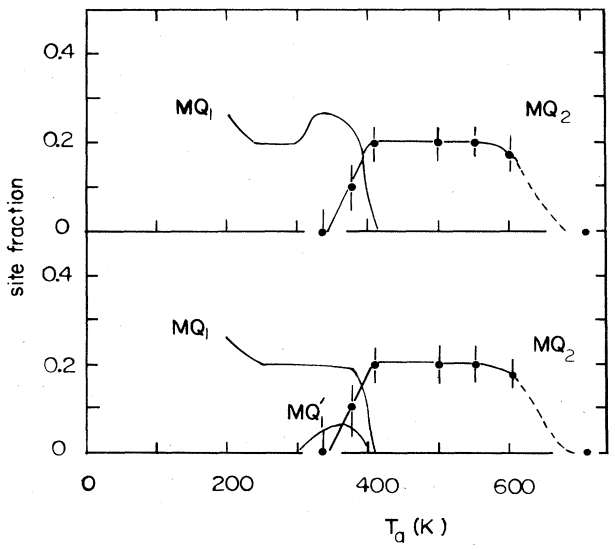


FIG. 5. Two plausible schemes for breaking the combined-interaction sites into components for the Ni sample irradiated with 1.5-MeV protons at 200 K to a dose of $17 \times 10^{15} p/\text{cm}^2$. The data points are the site fractions of $MQ_2$ obtained by fitting the signals to a Gaussian decay. The sum of drawn lines in each panel represents the total combined-interaction fraction obtained by subtracting the pure magnetic signals from unity.

$MQ_1$ involves only one defect which traps athermally at low temperature and thermally in the range 320—380 K [Fig. 5(a)]. The second assumes that $MQ_1$ involves two distinct complexes, one which forms athermally at low temperature and another which traps thermally at 320—380 K [Fig 5(b)]. It is not possible to distinguish the two cases from the available data.

(6) The $\sim 20\%$ of $^{111}$In atoms found in undetectable sites before irradiation appears to remain undetectable after subsequent irradiation and annealing to 700 K. The most plausible explanation for these permanently missing sites appears to involve grain boundaries or dislocation structures which do not change during irradiation or annealing.

### B. Deformed Ni

Samples, 25-$\mu$m-thick, consisting of 99.998%-pure polycrystalline Ni foils, were doped with $^{111}$In as described above. Deformation was done using a jeweler's roller either at room temperature or at 200 K when immersed in a mixture of methanol and solid $CO_2$. The dose of deformation was characterized by the increase in the sample area and ranged from 6% to 190%. Isochronal annealing studies were performed after different deformations, in the same way as for the irradiated samples. One PAC spectrum was obtained above the Curie temperature in a vacuum of $10^{-6}$ Torr with no applied magnetic field [see Fig. 1(b)].

As for the irradiated samples, the PAC spectra showed four different signals: The substitutional and C site, and two combined-interaction signals with decay times $\Delta$ of $\sim 5$ and $\sim 7$ ns, henceforth referred to as $MQ_1$ and $MQ_3$. Whereas we identify the short decay site with a similar site found after irradiation, neither of the combined sites are well-defined, and both could involve a superposition of different sites.

Site fractions are plotted in Fig. 2(b) for a sample deformed to 20% area increase at 200 K. As in Fig. 2(a), solid lines represent the amplitudes of the directly measured magnetic signals, and the dashed line the sum of the combined-interaction sites obtained by subtraction. The decay time $\Delta$ for combined-interaction sites is shown in Fig. 3(b), and several dose dependences of trapping behaviors are given in Fig. 6. Examination of these figures leads to the following observations.

(1) As for irradiated samples, the C site forms thermally in the range 325—400 K and dissolves at 600—650 K [Fig 2(b)]. The maximum C site population, observed for annealing temperatures in the range $400 < T_a < 600$ K, increases with dose up to about 30% area increase, and then levels off [Fig. 6(a)]. With increasing dose, the formation temperature of the C site shifts downward by as much as 12 K (not shown), as would be expected if the number of jumps needed for defect trapping decreases.

(2) The combined-interaction site $MQ_1$, characterized by a mean decay time of $\sim 5$ ns, forms athermally during deformation above a threshold of 10% area increase [Fig. 6(b)], and transforms or detraps in the range 370—420 K; unlike the irradiated sample, however, additional trapping occurs between 200 and 350 K, possibly due to enhanced diffusion along dislocation lines. A similar effect has

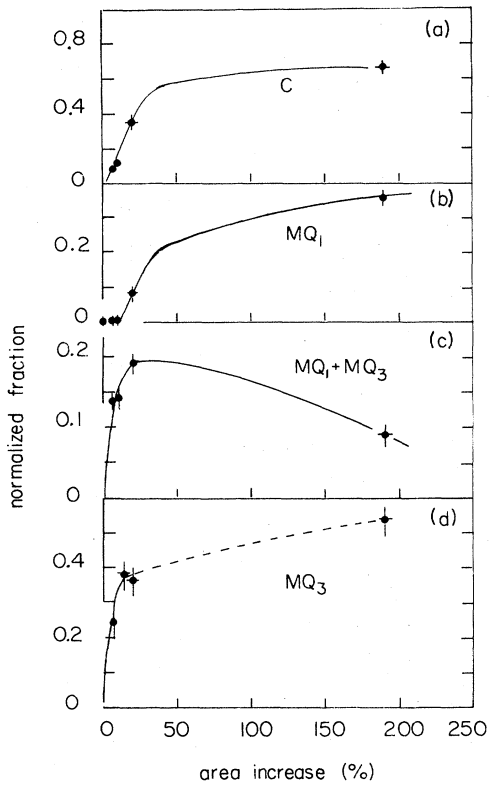


FIG. 6. Damage-dose plots for polycrystalline Ni samples deformed at 200 K. (a) Maximum C-site fraction achieved throughout the annealing sequence, normalized by the defect-free fraction at 300 K. (b) $MQ_1$ fraction produced by deformation at 200 K, normalized by the defect-free fraction before deformation. (c) The increase in the combined-interaction fraction upon annealing from room temperature to the temperature where the combined-interaction fraction is maximum, normalized by the defect-free fraction at room temperature. This quantity characterizes the trapping behavior of $MQ_1$ and $MQ_3$ between 300 and about 380 K (see text). (d) $MQ_3$ fraction at 500 K normalized by the defect-free fraction before deformation.

been observed for Al by Müller[40] using PAC and by Sassa *et al.*[41] using Mössbauer spectroscopy. As in the case of irradiation there is evidence that the athermal formation of $MQ_1$ does not saturate until large doses are reached [Fig. 6(b)].

(3) The combined-interaction site $MQ_3$, characterized by a mean decay time $\Delta\sim 7$ ns, forms in the range 350—420 K, and appears to replace $MQ_1$. A measurement above the Curie temperature (631 K) showed $MQ_3$ to have a mean quadrupole interaction frequency of $\omega_0=67(8)$ Mrad/s and a frequency distribution width $\sigma_Q=15$ Mrad/s [Fig. 1(b)]. Subsequent measurements at $T=295$ K showed no change in $\Delta$, indicating that $MQ_3$ persists to above $T_C$ and therefore has high thermal stability. The dissociation temperature of $MQ_3$ was 750—850 K after light deformation, but decreased gradually as the dose was increased, becoming about 650 K after heavy deformation. This may be understood as thermal detrapping at low dose and premature dissociation at high dose due to recrystallization. (It is known that heavily deformed Ni recrystallizes at a lower temperature than less heavily deformed material.[42])

(4) For samples deformed below 20% area increase, the combined-interaction sites show a thermal trapping stage between 340 and 375 K, whereas for deformations larger than 80% this stage can not be distinguished from a gradual trapping stage extending from 200 to 400 K. Figure 6(c) demonstrates that the mixed-interaction site population that forms thermally at 340—375 K saturates rapidly with increasing dose, as in the case of irradiated samples.

(5) As after irradiation, decomposition of the combined-interaction sites is ambiguous because it is not clear that the site $MQ_1$ formed athermally at 200 K is the same as the mixed-interaction site formed thermally at 340—375 K.

(6) Just as for irradiated Ni, $\sim$20% of the $^{111}$In atoms which are undetectable before deformation remain so after deformation and annealing to 900 K.

### C. Comparison to ion implantation

It is interesting to compare the results of the present work to earlier data for which initial damage consisted of collision cascades surrounding implanted $^{111}$In atoms. In work published in 1977,[21] only the substitutional, C-site, and $B_1$-site populations were analyzed, with results shown in Fig. 2(c). More recently, samples implanted at 77 or 295 K permitted distinction between combined-interaction signals observed below and above stage III [Fig. 3(c)].[43] Overall, as shown in Figs. 2 and 3, implantation results are found to be quite similar to the present work on irradiation and deformation, and lead to the following comparative findings.

(1) The C site appears after all three ways of damaging with essentially the same trapping and detrapping temperatures.

(2) The $MQ_1$ site appears through athermal trapping at low temperature in all three cases. After ion implantation or proton irradiation, $MQ_1$ also has a clearly defined thermal trapping stage at 270—350 and 320—380 K, respectively, followed by dissolution or transformation in the range 380—410 K. After deformation or ion implantation there is, in addition, a continuous increase in $MQ_1$ over a broad range of temperatures below 300 K, suggesting enhanced diffusion of defects in damage zones.[40,41]

(3) After proton irradiation or deformation new combined-interaction sites appear in the range of temperatures in which $MQ_1$ is observed to dissociate. In measurements below $T_C$, it takes the form $MQ_2$ or $MQ_3$ after proton irradiation and deformation, respectively, with decay times $\Delta\sim 12$ or $\Delta\sim 7$ ns, respectively. The same transition in decay times is suggested by the (incomplete) implantation data [see Fig. 3(c)], with the combined-interaction site taking the form $B_1$ when measured above $T_C$ but having a decay time $\Delta\sim 9$ ns when measurements are made at $T=295$ K. In measurements above $T_C$, $MQ_3$ has frequency $\omega_0=67(8)$ Mrad/s and distribution width 15(3) Mrad/s, partially overlapping the frequency $\omega_0=53(5)$ Mrad/s and width 8(2) Mrad/s observed for

$B_1$.[21] In the following we designate $B_1$ the site which has the parameters listed in Table I when measured above $T_C$ and $\Delta \sim 9$ ns when measured at room temperature.

(4) After all methods of damaging, no evidence of free migration and trapping was observed above 410 K. (The slight growth and decay of the mixed-interaction site fraction near 600 K is believed to result from partial breakup of the cubic trivacancy trap.)

## IV. INTERPRETATION

The PAC results we have described may be compared to resistivity recovery stages outlined in Table I and illustrated for electron-irradiated Ni in Fig. 7.[44] Whereas stages I and III are both attributed to free migration of defects, the focus of the present study is stage III (only the implantation data span stage I, and show no trapping there).

Free migration in stage III has been given two alternative interpretations, one based on a second interstitial species,[45–48] the other on vacancies.[7,49–51] The vacancy character of stage III appears to be more strongly supported for most fcc metals. Some of the supporting data have been cited in Table I, and various arguments are summarized in the review article by Balluffi.[52] For Ni, perhaps the best single argument is based on the lack of any free-migration stage above stage III in resistivity experiments where samples were damaged by low-dose electron irradiation: this indicates that vacancies *must migrate in stage III* if stage I is attributed to interstitials.

Assigning a vacancy character to stage III in Ni leaves

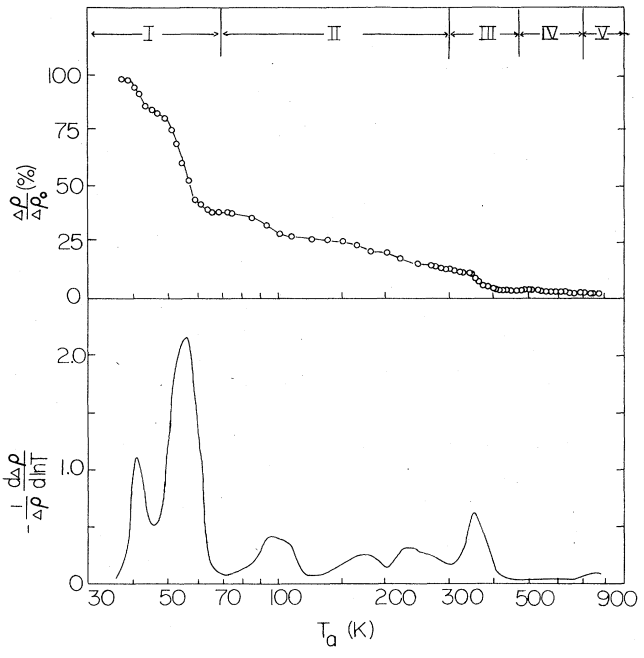


FIG. 7. Isochronal resistivity recovery curve (top) for electron-irradiated Ni with its numerical derivative (bottom), measured by Khanna and Sonnenberg (Ref. 44). The approximate ranges of the resistivity recovery stages in Ni are indicated in the top panel.

open the question of which vacancy defects are involved and how. Previous PAC studies already summarized in Table II have established a partial answer to this question:

(1) The cubic site C is interpreted as a trivacancy trap in which an $^{111}$In atom has relaxed to the center of a tetrahedron of vacancy lattice sites,[21] a structure that conforms to ion-channeling experiments[15,16] and computer calculations.[23,53] For deformed samples Collins and Schuhmann[20,26] find that this site forms predominantly via direct trapping of migrating trivacancies on substitutional $^{111}$In, and not via multiple trapping of smaller vacancy clusters.

(2) The noncubic site $B_1$, with the principal component of the electric field gradient in the $\langle 111 \rangle$ direction, is believed to be either a divacancy trap or a vacancy loop of variable size with formation temperature variously specified as 280 K (Ref. 1) or 550 K (Ref. 21). The vacancy-loop structure was proposed for similar complexes in Ni, Cu, and Au.[54]

(3) The high-frequency combined-interaction site, corresponding to $MQ_1$ in the present work, has unclear formation and dissolution temperatures, and several possible interpretations.

The present measurements monitor the site C, distinguish four combined-interaction sites, $MQ_1$, $MQ_2$, $MQ_3$, and $B_1$, via different decay times $\Delta$, and survey isochronal annealing and dose-dependent behavior for each. This leads to an extension of previous work in the following ways.

(1) The observation of thermal formation of site C already after low-dose proton irradiation (a situation expected only to produce small vacancy clusters) confirms the earlier hypothesis that site C involves at most a few vacancies.

(2) The C-site population saturates at higher doses than those needed to saturate the $MQ_1$ populations, implying that the latter must involve even fewer vacancies.

(3) Athermal and thermal formation of site $MQ_1$ after all three methods of damaging further suggests that simple, common defects are involved.

(4) It is possible to assign rough values for the coupling frequencies of $MQ_1$, characterized by $\Delta \sim 5$ ns. For this, we compare $\Delta$ to widths of initial anisotropy decays computed by Pleiter *et al.* [see Fig. 1(a) of Ref. 39]. Assuming reasonably that $\omega_L$ for $MQ_1$ is less than 98 Mrad/s, the Larmor frequency of substitutional In, we deduce a value of $\omega_0$ in the range 100—150 Mrad/s. Whereas this signal is consistent with that expected for a near-neighbor monovacancy trap,[1] it could also involve more than one site. We can therefore envision the following alternatives to apply for all methods of damaging:

(a) $MQ_1$ arises only from athermal and thermal trapping of monovacancies at the probe site.

(b) Athermal formation of $MQ_1$ involves monovacancies, but thermal formation of $MQ_1$ (and observed enhanced diffusion) involves divacancy trapping.

(c) Monovacancies and divacancies are both involved in athermal and thermal formation of $MQ_1$.

Furthermore, we cannot exclude that the involvement of

monovacancies or divacancies in $MQ_1$ could differ between methods of damaging, or between low and high doses of damage.

The assignment of monovacancies to athermal formation of $MQ_1$ is supported by analogy to nonmagnetic fcc metals, for which implantation experiments systematically show athermal formation of monovacancy traps, but not other defect complexes.[1] The assignment of divacancies to enhanced diffusion or thermal trapping is suggested by the fact that divacancies have the lowest calculated migration energy in Ni,[22] and because divacancies have already been observed as enhanced diffusers after deformation in other fcc metals.[40,41,55] For these reasons, possibility (b) above seems the most plausible explanation of the observed behavior of $MQ_1$.

(5) The very high dissociation temperatures of sites $MQ_2$, $MQ_3$, and $B_1$ show that they are all highly stable complexes. Small vacancy clusters in fcc metals typically have much smaller binding energies with In (Refs. 1 and 20) ($\sim$0.2 eV) than would be inferred from the present measurements ($\sim$1 eV). Therefore, all three sites are likely to involve larger defect clusters. A common origin is suggested by the fact that all three sites are observed to form near 400 K, the temperature at which $MQ_1$ dissociates, and from the measurements of $MQ_3$ and $B_1$ above $T_C$, indicating an overlap between the distributions of $\omega_0$. The different values of $\Delta$ and the different detrapping temperatures of $MQ_2$, $MQ_3$, and $B_1$ are then understood in terms of the eventual size of the resulting defect clusters.

## V. CONCLUSION

Based on a comparative analysis of PAC data for irradiated, deformed, and implanted $Ni^{111}In$, we arrive at a plausible model for vacancy trapping and migration in or below stage III. The model includes the following features.

(i) Monovacancies trap athermally at low temperature after all methods of damaging to form a combined-interaction state, $MQ_1$.

(ii) For high doses of damage, as occurs for heavily deformed and implanted samples, $MQ_1$ forms through enhanced diffusion of divacancies below 300 K.

(iii) Monovacancies and/or divacancies migrate, trap, and cluster in the range 320—380 K for irradiated and deformed samples, and 270—350 K for implanted samples, forming four combined-interaction sites, $MQ_1$, $MQ_2$, $MQ_3$, and $B_1$, and possibly the cubic C site.

(iv) Trivacancies, formed directly by the damaging process, or through accretion of monovacancies and divacancies, migrate and trap to form the C site in the range 320—400 K for irradiated and deformed samples, and 280—400 K for implanted samples.

(v) Whereas $MQ_1$ always dissociates in the range 380—450 K, implying a detrapping process, $MQ_2$, $MQ_3$, $B_1$, and C all have high thermal stability and dissolve in the range 600—850 K.

Stage-III recovery in Ni therefore involves at least two, and possibly three, freely migrating vacancy defects.

## ACKNOWLEDGMENTS

The authors wish to thank Dr. Raymond Goloskie of Worcester Polytechnic Institute for assistance in the proton irradiation. This material is based upon work supported by the National Science Foundation under Grant No. 81-08307.

*Present address: Department of Physics, Washington State University, Pullman, WA 99164.

[1]F. Pleiter and C. Hohenemser, Phys. Rev. B **25**, 106 (1982).
[2]E. Recknagel, G. Schatz, and Th. Wichert, in *Topics in Current Physics, Vol. 31: Hyperfine Interactions of Radioactive Nuclei,* edited by H. Christiansen (Springer-Verlag, New York, 1983), p. 133.
[3]Th. Wichert, Hyperfine Interact. **15-16**, 335 (1983).
[4]L. Niesen, Hyperfine Interact. **10**, 619 (1981).
[5]Carl Allard, Gary S. Collins, and Christoph Hohenemser, Hyperfine Interact. **15-16**, 387 (1983).
[6]A. van den Beukel, in *Vacancies and Interstitials in Metals,* edited by A. Seeger, D. Schumacher, W. Schilling, and J. Diehl (North-Holland, Amsterdam, 1970), p. 427.
[7]W. Schilling and K. Sonnenberg, J. Phys. F **3**, 322 (1973).
[8]W. Wycick and M. Feller-Kniepmeier, J. Nucl. Mater. **69-70**, 616 (1978).
[9]O. Bender and P. Ehrhart, J. Phys. F **13**, 911 (1983).
[10]H. Kronmüller, in *Vacancies and Interstitials in Metals,* Ref. 6, p. 667.
[11]D. Werneth, Phys. Status Solidi A **46**, 99 (1978).
[12]K.-H. Robrock, in *Point Defects and Defect Interactions in Metals,* edited by J. Takamura, M. Doyama, and M. Kiritani (University of Tokyo Press, Tokyo, 1982), p. 353.
[13]M. H. Yoo and J. O. Stiegler, J. Nucl. Mater. **69-70**, 813 (1978).
[14]K. Urban, in *Fundamental Aspects of Radiation Damage in Metals,* edited by M. T. Robinson and F. W. Young (U.S. Department of Commerce, Springfield, VA, 1975), p. 675.
[15]L. M. Howe, M. L. Swanson, and A. F. Quenneville, Nucl. Instum. Methods **218**, 663 (1983).
[16]M. L. Swanson and L. M. Howe, Nucl. Instrum. Methods, **218**, 613 (1983).
[17]M. L. Swanson, L. M. Howe, and A. F. Quenneville, J. Nucl. Mater. **69-70**, 372 (1978).
[18]G. Dlubek, O. Brümmer, and P. Sickert, Phys. Status Solidi A **39**, 401 (1977).
[19]G. Dlubek, O. Brümmer, N. Meyendrof. P. Hautojärvi, A. Vehanen, and J. Yli-Kauppila, J. Phys. F **9**, 1961 (1979).
[20]Gary S. Collins and Reinhardt B. Schuhmann, Hyperfine Interact. **15-16**, 391 (1983).
[21]C. Hohenemser, A. R. Arends, H. de Waard, H. G. Devare, F. Pleiter, and S. A. Drentje, Hyperfine Interact. **3**, 297 (1977).
[22]R. A. Johnson, Phys. Rev. **152**, 629 (1966).
[23]A. G. Crocker in *Interatomic Potentials and Crystalline Defects,* edited by Jong K. Lee (Metallurgical Society of AIME, Warrendale, Penn., 1981), p. 87.
[24]K. -H. Robrock, J. Phys. (Paris) Colloq. **42**, C5-709 (1981).

[25]C. Allard, Ph. D. thesis, Clark University, 1985.
[26]Gary S. Collins and Reinhardt B. Schuhmann (unpublished).
[27]A. Andreeff, H. -J. Hunger, and S. Unterricker, in *Hyperfine Interactions Studied in Nuclear Reactions and Decay, Contributing Papers,* edited by E. Karlsson and R. Wäppling (University of Uppsala Press, Uppsala, 1974), p. 68.
[28]C. Hohenemser, A. R. Arends, and H. de Waard, Phys. Rev B **11**, 4522 (1975).
[29]F. Namavar, M. Rots, J. Claes, and R. Coussement, Hyperfine Interact. **12**, 233 (1982).
[30]R. M. Suter, M. Haoui, and C. Hohenemser, Hyperfine Interact. **4**, 711 (1978).
[31]C. Allard, G. S. Collins, and C. Hohenemser, in *Electronic Structure and Properties of Hydrogen in Metals,* edited by P. Jena and C. B. Satterthwaite (Plenum, New York, 1983), p. 589.
[32]Gary Scott Collins, Gil P. Stern, and Christoph Hohenemser, Phys. Lett. **84A**, 289 (1981).
[33]F. Pleiter, Hyperfine Interact. **4**, 710 (1978).
[34]A. R. Arends, H. Hasper, C. Hohenemser, J. G. Mullen, G. van Opbroek, and F. Pleiter, Hyperfine Interact. **10**, 659 (1981).
[35]H. Frauenfelder and R. M. Steffen, in *Alpha-, Beta-, and Gamma-Ray Spectroscopy,* edited by K. Siegbahn (North-Holland, Amsterdam, 1966), p. 997.
[36]*The Electromagnetic Interaction in Nuclear Spectroscopy,* edited by W. D. Hamilton (North-Holland, Amsterdam, 1975).
[37]M. J. L. Yates. in *Alpha-, Beta-, and Gamma-Ray Spectroscopy,* Ref. 35, Appendix 9.
[38]A. R. Arends, C. Hohenemser, F. Pleiter, H. de Waard, L. Chow, and R. M. Suter, Hyperfine Interact. **8**, 191 (1980).
[39]F. Pleiter, A. R. Arends, and H. G. Devare, Hyperfine Interact. **3**, 87 (1977).
[40]H. G. Müller, Z. Phys. B **47**, 119 (1982).
[41]K. Sassa. W. Petry, and G. Vogl, Philos. Mag. A **48**, 41 (1983).
[42]*Recrystallization of Metallic Materials,* edited by F. Haessner (Riederer-Verlag, Stuttgart, 1971).
[43]F. Pleiter and C. Hohenemser (unpublished).
[44]S. K. Khanna and K. Sonnenberg, Radiat. Eff. **59**, 91 (1981).
[45]W. Frank and A. Seeger, Cryst. Lattice Defects **5**, 141 (1974).
[46]W. Frank and A. Seeger, Radiat. Eff. **25**, 17 (1975).
[47]A. Seeger, in *Vacancies and Interstitials in Metals,* Ref. 6, p. 999.
[48]A. Seeger, in *Fundamental Aspects of Radiation Damage in Metals,* Ref. 14, p. 493.
[49]W. Schilling, G. Burger, K. Isebeck, and H. Wenzl, in *Vacancies and Interstitials in Metals,* Ref. 6, p. 255.
[50]W. Schilling, P. Ehrhart, and K. Sonnenberg, in *Fundamental Aspects of Radiation Damage in Metals,* Ref. 14, p. 470.
[51]W. Schilling, J. Nucl. Mater. **69-70**, 465 (1978).
[52]R. W. Balluffi, J. Nucl. Mater. **69-70**, 240, (1978).
[53]A. C. Damask and G. J. Dienes, Phys. Rev. **113**, 781 (1959).
[54]M. Deicher, O. Echt, E. Recknagel, and Th. Wichert, Hyperfine Interact. **10**, 667 (1981).
[55]M. L. Swanson, Th. Wichert, L. M. Howe, A. F. Quenneville, and O. M. Westcott, in *Advanced Photon and Particle Techniques for the Characterization of Defects in Solids,* edited by J. B. Roberto (Materials Research Society, Pittsburgh, Penn., 1984), p. 35.